Journal of Molecular Graphics and Modelling 28 (2009) 357–367

Contents lists available at ScienceDirect

Journal of Molecular Graphics and Modelling

journal homepage: www.elsevier.com/locate/JMGM

3D-QSAR analysis of cycloguanil derivatives as inhibitors of A16V + S108T mutant *Plasmodium falciparum* dihydrofolate reductase enzyme

Legesse Adane, Prasad V. Bharatam *

Department of Medicinal Chemistry, National Institute of Pharmaceutical Education and Research (NIPER), S.A.S. Nagar 160 062, Punjab, India

ARTICLE INFO

Article history:
Received 30 June 2009
Received in revised form 27 August 2009
Accepted 1 September 2009
Available online 6 September 2009

Keywords:
*Pf*DHFR
CoMFA
CoMSIA
3D-QSAR
1,3,5-Triazine

ABSTRACT

A three-dimensional quantitative structure–activity relationship (3D-QSAR) study was carried out on cycloguanil derivatives which are reported as growth inhibitors of *Plasmodium falciparum* clone (T9/94 RC17) which harbors A16V + S108T mutant dihydrofolate reductase (DHFR) enzyme. Comparative of Molecular Field Analysis (CoMFA) and Comparative of Molecular Similarity Indices Analysis (CoMSIA) were carried out to investigate the structural requirements for the activities of these compounds and to derive predictive models that may be used for designing novel *Pf*DHFR enzyme inhibitors. The global minimum energy (within the search space) conformation of the most active compound (**38**) was obtained by using simulated annealing, and was subsequently used as a template to build the structures of the rest molecules used in the study. The CoMFA model gave statistically significant results with r^2_{cv} and r^2_{ncv} values of 0.654 and 0.951, respectively. The combination of steric, electrostatic and hydrophobic fields resulted in the best CoMSIA model with r^2_{cv} and r^2_{ncv} values of 0.669 and 0.907, respectively. The predictive abilities of the CoMFA and CoMSIA models were also evaluated using test compounds which gave r^2_{pred} values of 0.735 and 0.557, respectively. The results of bootstrapping analyses also confirmed that the generated models are robust and reliable. The models were graphically interpreted using CoMFA and CoMSIA contour plots. The structural regions responsible for the differences in anti-plasmodial activities were analyzed with respect to their electrostatic, steric and hydrophobic nature. The results obtained from this study could be used for rational design of potent inhibitors against A16V + S108T mutant *Pf*DHFR enzyme.

1. Introduction

Malaria is one of the most prevalent diseases in tropical and sub-tropical regions of the world. It causes 300–500 million clinical cases and 1.5–3 million deaths annually in tropical regions [1–7]. In addition to health-related problems, malaria also causes economic burden on patients and countries where it is prevalent [8]. *Plasmodium falciparum* is the most dangerous causative agent which is responsible for the majority of morbidity and mortality cases associated with malaria. The widespread occurrence of malaria could be attributed to the development of resistance of the parasite to the available antimalarial drugs such as chloroquine, cycloguanil and pyrimethamine. These drugs have long been used clinically in the treatment of malaria infection, especially to *P. falciparum* malaria. However, their clinical utilization has been compromised due to the emergence of drug-resistant parasite in many countries [3,5,9–14]. Therefore, new and effective drugs are urgently needed for malaria treatment.

The dihydrofolate reductase (DHFR) domain of a bifunctional enzyme which is known as dihydrofolate reductase-thymidylate synthase (DHFR-TS) is one of the well-established drug targets in *P. falciparum*. It catalyzes NADPH-dependent reduction of 7,8-dihydrofolate (DHF) to 5,6,7,8-teterahydrofolate (THF) that plays a crucial role in many biochemical processes such as folate metabolism and DNA synthesis. Thus, inhibition of DHFR causes interruption of DNA formation which ultimately results in death of the parasitic cells. This observation has been exploited to design antimalarial agents that inhibit the normal function of *Pf*DHFR enzyme [15–23]. It is a specific target for type-2 antifolates such as pyrimethamine and cycloguanil [17,18,24–26]. These antimalarial drugs selectively inhibit *Pf*DHFR enzyme without affecting the corresponding enzyme in humans. However, due to point mutations at amino acid residues 16, 51, 59, 108 and 164 in the active site of *Pf*DHFR enzyme, the therapeutic values of cycloguanil and pyrimethamine have dramatically declined in many parts of the world [27,28]. Such mutations decrease the optimal binding interactions of the drugs and amino acid residues in the active site of *Pf*DHFR enzyme which result in reduction of efficacy [26,29–31].

Computer-aided drug design approaches such as pharmacophore mapping [32,33], docking [33,34], homology modelling

* Corresponding author. Tel.: +91 1722214682/87; fax: +91 1722214692.
E-mail address: pvbharatam@niper.ac.in (P.V. Bharatam).

1093-3263/$ – see front matter © 2009 Elsevier Inc. All rights reserved.
doi:10.1016/j.jmgm.2009.09.001

[19–21,29–31,35–36] and quantitative structure–activity relationships (QSAR) models [37–40] are some of the approaches which have been employed in understanding parasitic drug resistance, and also in designing antimalarial drug candidates for inhibition of drug-resistant *P. falciparum* parasite. QSAR models are used to correlate chemical structures to biological activities. These methodologies are used to predict properties such as binding affinities, toxicity (QSRT), absorption, disposition, metabolism and excretion (ADME) of drug candidates (including yet unsynthesized ones), and are also used for lead discovery and optimization [41–44]. Three-dimensional quantitative structure–activity relationships (3D-QSAR) models are used to analyze favorable and unfavorable pharmacophoric features of molecules which play a crucial role in the interaction of ligands with a particular protein target. In such cases the physicochemical properties of compounds, which are represented in the form of molecular interaction fields, are correlated with *in vivo* or *in vitro* activity data. Two of the most widely used 3D-QSAR approaches are based on Comparative Molecular Field Analysis (CoMFA) [45] and Comparative Molecular Similarity Index Analysis (CoMSIA) [46]. In CoMFA model, the steric and electrostatic fields are computed based on 3D-structures of ligands in the training set. The calculated fields are correlated with experimental biological activity data by Partial Least Square (PLS) analysis to derive 3D-QSAR models. Different color-coded contour maps surrounding the ligands give insights about favorable and unfavorable ligand–receptor interactions, and also used as guides for designing novel leads. On the other hand, CoMSIA model calculates similarity indices around the molecules using physicochemical properties such as steric, electrostatic hydrogen bond donor, hydrogen bond acceptor and hydrophobicity [46].

There are several literature reports on QSAR models developed for the purpose of understanding *Pf*DHFR enzyme–inhibitor interactions and mechanism of drug-resistance by *P. falciparum* parasite towards cycloguanil and pyrimethamine [38–40]. Maitarad et al. carried out 3D-QSAR/CoMFA and 3D-QSAR/CoMSIA studies using cycloguanil analogs against wild type and quadruple mutant *Pf*DHFR enzymes [47]. Recently, they also reported the result CoMFA and CoMSIA studies based on pyrimethamine derivatives active against quadruple mutant type *Pf*DHFR enzyme [48]. To the best of our knowledge, no 3D-QSAR studies have been carried out based on the reported activities of cycloguanil derivatives against A16V + S108T mutant *Pf*DHFR enzyme. This prompted us to generate 3D-QSAR models using the title compounds for which their growth inhibition activities against *P. falciparum* clone (T9/94 RC17) harboring A16V + S108T mutant DHFR enzyme are reported in the literature [35,36]. In this report we present the results of our study.

2. Materials and methods

2.1. Data set

A data set of 42 cycloguanil derivatives was used as input data for the 3D-QSAR study [35,36]. The compounds were evaluated for their *in vitro* anti-plasmodial activities of cycloguanil-resistant *P. falciparum* clone harboring A16V + S108T mutant *Pf*DHFR enzyme. These activity tests were carried out by the same research team and also the same biological assay methods [35,36]. The growth inhibition constant (IC_{50}) values, i.e., the concentration of inhibitor required for 50% growth inhibition were converted into pIC_{50} using the formula $pIC_{50} = -\log IC_{50}$. pIC_{50} values were then used as dependent variables for generation of the CoMFA and CoMSIA analyses. The reported IC_{50} values are given in the original literatures [35,36], and they were used without considering the reported experimental errors. The selection of the training and test sets which contain 32 and 10 compounds was performed randomly. The pIC_{50} values of the training set compounds range from 4.18 to 8.40 which was also believed to contribute for the suitability of the training set compounds for the 3D-QSAR study.

2.2. Molecular modelling

All molecular modelling studies were carried out using SYBYL6.9 installed on a Silicon Graphics Octane2 workstation running with IRIX6.5 operating system [49]. Since no bound ligand or crystal structure of A16V + S108T mutant *Pf*DHFR enzyme was available, the lowest energy conformer of the most active compound (**38**) was used as a template for proposition of the bioactive conformation. This is a common approach in ligand-based 3D-QSAR studies in the absence of 3D-structural information of the receptor or enzyme [50–55]. A preliminary minimization was performed on **38** to remove close atom or bad van der Waals contacts by using 1000 cycle minimization with standard Tripos force field. A 0.005 kcal/mol energy gradient convergence criterion using Powell's method was also used as a final step of energy minimization. To obtain the lowest energy conformer, **38** was then subjected to simulated annealing to heat the molecule at 700 K for 1000 fs followed by anneal the molecule to 200 K for 1000 fs [54,56]. The resulting conformer with the lowest potential energy was saved and subsequently used as a template. All the remaining molecules were constructed based on this template, and subjected to 1000 cycle minimization with the standard Tripos force field and 0.005 kcal/mol Å energy gradient convergence criterion using Powell's method. All the molecules were assigned with Gasteiger–Huckle charges [57].

2.3. Molecular alignment

Development of CoMFA model is alignment-sensitive. Therefore, due precaution is required during the molecular alignment step of development of this model. There are different types of alignments. These are (i) atom-fit, (ii) data base alignment, (iii) binding-site guided or docking alignment procedure and (iv) field-fit alignment [45,58]. In this study an atom-fit alignment method was used to align molecules. The lowest energy conformer of the most active compound (**38**) was used as a template for the alignment. But before using **38** as a template, its alignment was validated by superimposing on the X-ray conformation of pyrimethamine extracted from double mutant (1J3J.pdb) *Pf*DHFR [23].

2.4. 3D-QSAR model generation

2.4.1. CoMFA model generation

A Comparative Molecular Field Analysis (CoMFA) was carried out to evaluate steric and electrostatic fields using the QSAR module, and was scaled using the CoMFA standard in SYBYL6.9 [49]. All the analyses were performed by placing aligned training set molecules in a 3D grid with a spacing of 2.0 Å. The van der Waals potential and Coulombic terms which represent steric and electrostatic fields, respectively, were calculated using the standard Tripos force fields. An sp^3 hybridized carbon was used as a probe atom to generate the steric (Lennard–Jones potential) field and a charge of +1.0 to generate the electrostatic (Coulomb potential) field. The steric and electrostatic contributions were set at a default cutoff energy value of 30 kcal/mol. Several CoMFA models were developed by permutation of molecules between training and test sets.

2.4.2. CoMSIA model generation

The Comparative Molecular Similarity Analysis (CoMSIA) model was developed in SYBYL 6.9 using training and test sets used in the

CoMFA model that gave the highest r^2_{cv} and r^2_{pred}. The statistical analyses of the CoMSIA model were performed in the same way as used for the CoMFA model. The standard value of 0.3 was used for the attenuation factor (α) which controls the steepness of the Gaussian function. Different combinations of steric, electrostatic, hydrophobic, H-bond donor and H-bond acceptor fields were used. All fields were also used at the same time in CoMSIA model generation.

2.5. Partial Least Square (PLS) analysis

This is a statistical method used to correlate CoMFA and CoMSIA fields with biological activities of compounds [45,59]. In this study the cross-validation (r^2_{cv}) was carried out using leave-one-out (LOO) method which removes one compound from the data set, and its properties predicted from the model developed using the rest of compounds. In order to increase the speed of the analyses and to improve noise-to-signal ratio, all the cross-validations were performed using a column filter value (δ) of 2.0 kcal/mol by omitting those lattice points whose energy variation is below this threshold value. After obtaining an optimum number of components in the cross-validation analysis step, a final non-cross validated analysis was performed using the optimal number of components obtained from LOO cross-validation step. The final CoMFA and CoMSIA models were selected based on criteria such as high r^2_{cv}, r^2_{ncv}, r^2_{pred}, and the small standard error of estimation (SEE) value. In order to evaluate the robustness and statistical validity of the derived models, bootstrapping (r^2_{bs}) was carried out for 100 runs and column filtering at 2.00 kcal/mol. This involves generation of many new data sets (also known as bootstrap samplings) from the original data set. These new data sets are of equal size with that of original ones and obtained by randomly choosing samples (rows) from the original data set. The statistical calculation is performed on each of these bootstrapping samplings. The difference between the parameters calculated from the original data set and the average of the parameters calculated from the many bootstrapping samplings is a measure of the bias of the original calculations. The entire cross-validated results were analyzed considering the fact that a value of r^2_{cv} above 0.3 indicates that probability of chance correlation is less than 5% [49,60,61].

2.6. Predictive ability of CoMFA and CoMSIA models

The predictive abilities of the generated models were evaluated using test set compounds that were not included in the training set. These molecules were included with the training set for alignment, and their activities were predicted using models derived using the training set. The predictive correlation (r^2_{pred}) was calculated using formula:

$$r^2_{pred} = \frac{SD - PRESS}{SD}$$

where SD is the sum of the squared deviations between the biological activities of the test set and mean activities of the training set compounds; PRESS is the sum of the squared deviations between the actual and predicted activities of the test compounds [45].

3. Results and discussion

3.1. Molecular alignment and model generation

The compounds selected for the 3D-QSAR analysis and their estimated biological activities are listed in Table 1. The chemical structures are given as supplementary information. Of 42 compounds used in the study, 32 molecules were included in the training set and the remaining 10 molecules were used as test set. The choice of compounds as training and test set was performed randomly. To validate the alignment of molecules, the lowest energy conformer of the most active compound (**38**) was superimposed on the conformation of pyrimethamine extracted from the active site of X-ray crystallographic structure of C59R + S108N mutant *Pf*DHFR. The result indicated that the 1,3,5-triazine ring and C6-alkyl side chain of **38** were found to superimpose on 2,4-diaminopyrimidine ring and 6-ethyl substituent of pyrimethamine, respectively (Fig. 1). The chlorophenyl substituents of **38** and pyrimethamine were not perfectly superimposed. The chlorophenyl substituent of the latter was slightly displaced above the plane of the corresponding substituent of **38**.

Table 1
Data set of compounds used for 3D-QSAR studies.

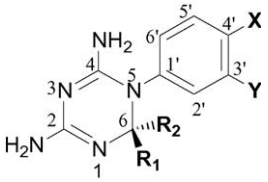

Compounds	R_1	R_2	X	Y	pIC_{50}
1	$-CH_3$	$-CH_3$	Cl	H	5.61
2	H	H	Cl	H	6.50
3	$-CH_3$	H	Cl	H	6.46
4	$-CH_2CH_3$	H	Cl	H	6.31
5[a]	$-CH_2CH_2CH_3$	H	Cl	H	6.64
6	$-CH_2(CH_2)_2CH_3$	H	Cl	H	6.60
7	$-CH(CH_3)_2$	H	Cl	H	5.55
8	$-C(CH_3)_3$	H	Cl	H	4.18
9[a]	$-C_6H_5$	$-CH_3$	Cl	H	7.36
10	$-CH_3$	$-CH_3$	Br	H	5.56
11	$-CH_3$	H	Br	H	6.56
12	$-CH_2CH_3$	H	Br	H	6.66
13[a]	$-CH_2CH_2CH_3$	H	Br	H	6.60
14	$-CH(CH_3)_2$	H	Br	H	6.14
15	$-C_6H_5$	H	Br	H	6.74
16	$-CH_3$	$-CH_3$	$-CH_3$	H	5.44
17	$-CH_3$	H	$-CH_3$	H	6.33
18	$-CH_2CH_3$	H	$-CH_3$	H	6.29
19[a]	$-CH_2CH_2CH_3$	H	$-CH_3$	H	6.82
20	$-CH(CH_3)_2$	H	$-CH_3$	H	5.46
21	$-C_6H_5$	H	$-CH_3$	H	7.41
22	$-CH_3$	$-CH_3$	H	H	6.35
23[a]	$-CH_3$	$-CH_3$	F	H	6.00
24	H	H	H	H	6.45
25	H	H	F	H	6.51
26[a]	$-CH_3$	$-CH_3$	H	Cl	6.53
27	$-CH_3$	$-CH_3$	Cl	Cl	6.51
28	$-CH_3$	H	H	Cl	7.55
29	$-CH_3$	H	Cl	Cl	7.72
30	$-C_6H_5$	H	H	Cl	7.62
31[a]	$-C_6H_5$	H	Cl	Cl	7.54
32	$-C_6H_4$-*p*-0-C_6H_5	H	Cl	H	7.40
33	$-C_6H_4$-*p*-O-C_6H_5	H	H	Cl	8.40
34	$-C_6H_4$-*m*-O-C_6H_5	H	H	Cl	7.22
35	$-C_6H_4$-*m*-$OCH_2C_6H_5$	H	H	Cl	6.72
36	$-C_6H_4$-*m*-(OC_6H_4-4′-Cl)	H	Cl	H	6.38
37[a]	$-C_6H_4$-m-(4′-ClC_6H_4)	H	H	Cl	6.41
38	*n*-C_7H_{15}	H	H	Cl	8.40
39[a]	$-C_6H_4$-*p*-OC_3H_7	H	H	Cl	8.40
40	$-C_6H_4$-*m*-(OC_6H_3-3′,5′-Cl	H	H	Cl	7.30
41	$-C_6H_4$-*m*-$O(CH_2)_2$ O(2′,4′,5′-Cl_3–C_6H_2)	H	H	Cl	6.43
42[a]	$-C_6H_4$-*m*-(3′-CF_3–OC_6H_4)	H	H	Cl	6.74

[a] Refers test set compounds.

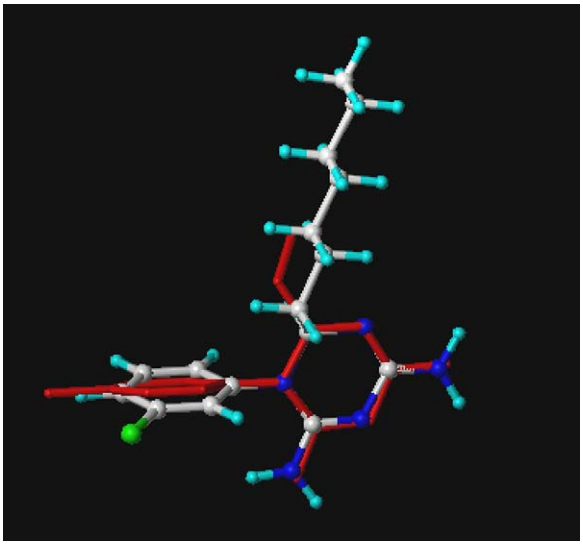

Fig. 1. The superimposition of the lowest energy conformer of **38** and X-ray crystallographic conformer of pyrimethamine extracted from double mutant *Pf*DHFR (1J3J.pdb). The conformer of pyrimethamine is shown in red.

This displacement could be attributed to a steric conflict between 4′-Cl group of pyrimethamine and the bulkier side chain of N108 (mutated from S108) in the mutant *Pf*DHFR (Section 3.2).

However, the observed superimposition (and small RMSD value of 0.178 Å) indicated that the lowest energy conformer of **38** could be used as a template. Then it was used as a template for an atom-fit alignment by choosing atoms N1–C6 and C1′–C6′ (Fig. 2). The aligned molecules were subsequently used to construct the CoMFA and CoMSIA models.

3.2. Statistical analyses

In our study, the CoMFA models were developed by random combination of compounds as training and test sets. Several models with high cross-validation coefficient (r^2_{cv}) and non cross-validation coefficient (r^2_{ncv}) values were generated (data not given). As pointed out by Golbraikh et al. [62] and Tropsha et al. [63], high correlation coefficient (r^2_{cv}) values of leave-one-out cross-validation are necessary but are not sufficient conditions to conclude whether a given model is reliable or not. They also suggested that use of an external test set as a method to validate reliability and

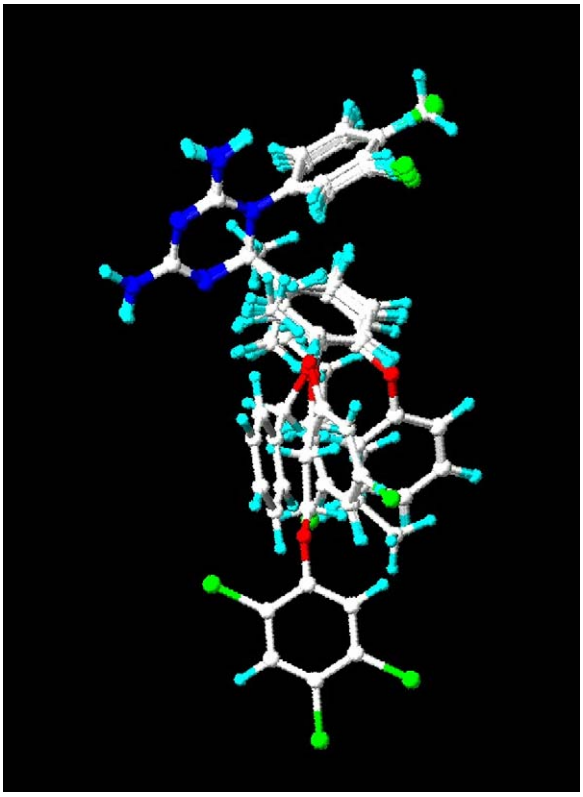

Fig. 2. Alignment of the training set molecules.

robustness of a model. Thus, the predictive abilities of all the generated models were evaluated by computing their predictive correlation coefficient (r^2_{pred}) using their respective test set compounds. The CoMFA model with the highest external predictive ability ($r^2_{pred} = 0.735$) was selected as the best model. The training set compounds used to generate this model, and the test set compounds are given in Table 1. The cross-validation coefficient, r^2_{cv}, and the non-cross validate coefficient, r^2_{ncv}, of this model were found to be 0.654 and 0.951, respectively, for optimum number of components (ONC) 7. The standard error of estimation (SEE) of this model was 0.222. The summary of statistics of the best CoMFA model is given in Table 2. The relative contributions of steric and electrostatic fields 76.7 and 23.3%, respectively, indicate that steric interactions are the major contributors for the variation

Table 2
Summary of CoMFA and CoMSIA statistics.

	CoMFA	CoMSIA								
	SE	SE	SED	SEA	SEH[a]	SEDA	SHDA	SEHD	SEHA	SEHDA
r^2_{cv}	0.654	0.650	0.592	0.614	0.669	0.591	0.657	0.661	0.652	0.654
r^2_{ncv}	0.951	0.902	0.915	0.916	0.907	0.915	0.951	0.934	0.934	0.934
ONC	7	6	7	6	6	6	12	8	8	8
r^2_{pred}	0.735	0.660	0.695	0.690	0.557	0.183	0.635	0.580	0.511	0.595
PRESS	1.390	1.810	1.600	1.630	2.318	4.274	1.912	2.200	2.570	2.120
F-value	66.64	38.45	45.07	45.22	40.77	45.07	30.92	40.72	40.88	40.98
SEE	0.222	0.308	0.286	0.286	0.300	0.286	0.249	0.264	0.263	0.263
Field contributions										
S	0.767	0.519	0.502	0.503	0.273	0.480	0.384	0.257	0.252	0.252
E	0.233	0.418	0.447	0.449	0.302	0.438	–	0.297	0.294	0.284
D	–	–	0.05	–	–	0.041	0.049	0.042	–	0.032
H	–	–	–	–	0.425	–	0.518	0.408	0.407	0.401
A		–	–	0.049	–	0.042	0.049	–	0.043	0.031

[a] Used for the final CoMSIA analysis; S: steric, E: electrostatic, D: H-bond donor, A: H-bond acceptor, and H: hydrophobic; r^2_{pred}: predictive correlation coefficient; ONC: optimum number of components; r^2_{cv}: cross-validated correlation coefficient; r^2_{ncv}: conventional correlation coefficient; SEE: standard error of estimation; *F*-value: *F*-test value; PRESS: predicted residual sum of squares of test set molecules.

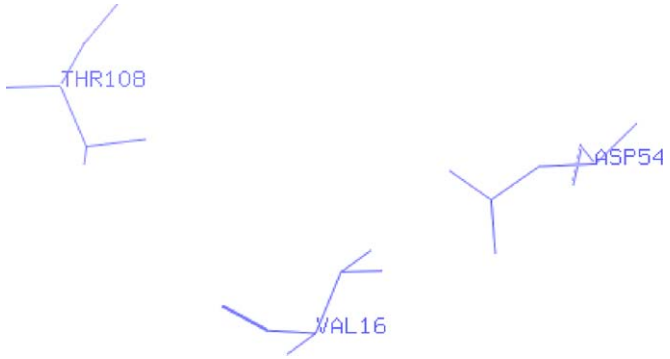

Fig. 3. The schematic representation of the relative orientations of Val16, Thr108 and Asp54 in the active site of A16V + S108T mutant *Pf*DHFR enzyme.

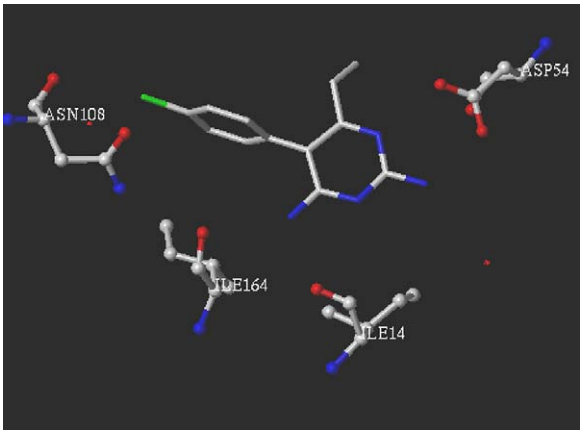

Fig. 4. The conformation of pyrimethamine bound in the active site of X-ray crystallographic structure of double mutant (S108N + C59R) *Pf*DHFR enzyme (1J3J.pdb).

of biological activities of cycloguanil derivatives used in the study. This observation is consistent with previous reports which suggested that steric interactions are mainly responsible for resistance of *P. falciparum* parasite to antimalarial drugs (e.g., cycloguanil and pyrimethamine). The point mutations S108N and A16V + S108T in the active site of *Pf*DHFR enzyme are associated with resistance to pyrimethamine and cycloguanil, respectively [26,29–31,35]. It has been hypothesized that the resistance to pyrimethamine is due to the steric interaction of the *para*-Cl group with the larger side chain of S108N mutant parasite. Similarly the steric clashes that exist (i) between the bulky amino acid residue (T108) and *para*-Cl group and (ii) between bulky amino acid residue (V16) and one of the methyl groups are known to be responsible for the resistance of A16V + S108T mutant *Pf*DHFR enzyme to cycloguanil [26,29–31,35]. These interactions cause displacement of these drugs from their optimal orientation in the active sites as compared to the corresponding orientation in the active site of wild type. Such displacements weaken the H-bond interaction between the drug molecules and the conserved aspartic acid residue (Asp54) which is crucial for inhibitory activity. Moreover, the steric clashes cause loss of the π-stacking interaction of the *p*-chlorophenyl groups of these drugs with the nicotine amide ring of NADPH. All these factors lead to reduction in the binding affinities and inhibitory activities of the drugs against the above mutant *Pf*DHFRs. The schematic representation showing the relative positions of V16, T108 and Asp54 in the active site of A16V + S108T mutant *P. falciparum* parasite is given in Fig. 3 whereas the conformation of pyrimethamine bound in the active site of X-ray crystallographic structure of double mutant (S108N + C59R) PfDHFR is shown in Fig. 4. As shown in Fig. 4, the *para*-chlorophenyl ring of pyrimethamine is displaced from a plane which is perpendicular to the plane of the 2,4-diaminopyrimidine ring. Similar displacement also occurs in the *para*-chlorophenyl ring of cycloguanil which results in loss of its binding interactions and affinity in the active site of A16V + S108T mutant enzyme as compared to that of the wild type. The steric factor due to the close proximity of the *para*-Cl group to bulky residue at 108 is the main reason for this displacement.

As indicated in Table 2, the predictive correlation coefficient ($r^2_{pred} = 0.735$) is reasonable to suggest that our model is a satisfactory model with good predictive ability. A high r^2 value (0.974) of bootstrapping which was carried out at 100 runs also supports the statistical validity of the model [54–56].

The CoMSIA models were also generated using the same molecular alignment and training set compounds which were used for the CoMFA model development. Since it is principally based only on standard steric and electrostatic molecular fields for predicting biological activities, CoMFA model does not provide adequate information regarding the binding interactions between substrates and active sites of enzymes. Therefore, CoMSIA model is usually used along with the conventional steric and electrostatic CoMFA model to get valuable information about such interactions by introducing three additional fields, viz. hydrophobic field, hydrogen bond donor- and hydrogen bond acceptor fields [49]. In this study, several combinations of physicochemical fields (steric, electrostatic, hydrophobic, H-bond donor, and H-bond acceptor) were used to generate CoMSIA models in order to examine the significance of each of these fields. Overall the contributions of hydrogen bond acceptor and donor fields to the CoMSIA models were not significant. In all the cases contributions of these fields were less than 5% whereas the contribution of hydrophobic field in all CoMSIA models containing this field was found to be significant. The contributions of these fields were 42.5, 51.8, 40.8, 40.7 and 40.1% in SEH, SHDA, SEHD, SEHA and SEHDA, respectively (Table 2). On the other hand, in those CoMSIA models containing steric and electrostatic fields, significant and similar contributions were observed from hydrogen bond acceptor and donor fields. Except for the SEDA model ($r^2_{pred} = 0.183$), all the generated CoMSIA models are statistically significant as demonstrated by their internal and external predictive abilities. The CoMSIA model generated by the combination of steric, electrostatic and hydrophobic fields was used for final analysis and prediction because of its acceptable statistical indices ($r^2_{cv} = 0.669$, $r^2_{ncv} = 0.907$, $r^2_{pred} = 0.557$ and $r^2_{bs} = 0.967$) which were obtained with lower number of principal components (ONC = 6). The steric, electrostatic and hydrophobic fields are in the ratio of 27.3, 30.2 and 42.5%, respectively. Use of additional fields (hydrogen bond donor and -acceptor fields) did not significantly improve the statistical indices as demonstrated in SEHDA CoMSIA model ($r^2_{cv} = 0.654$, $r^2_{ncv} = 0.934$ and $r^2_{pred} = 0.595$) (Table 2). The statistical indices of the selected CoMSIA-SEH model suggested that the model has good predictive ability. The summary of statistics of the CoMSIA studies is given in Table 2 along with the corresponding values of the best CoMFA model.

The comparison between the experimental and predicted activities of the training set (Table 3) and test set compounds (Table 4) indicated that both the COMFA and CoMSIA models show good predictive abilities. As demonstrated by the small residual values of both sets of compounds, the predicted pIC_{50} values were closer to the experimental pIC_{50} values. Fig. 5 shows the graph of predicted vs. experimental activities of the training and test set compounds. The linearity of the graphs also indicates that both the CoMFA (Fig. 5(a)) and CoMSIA (Fig. 5(b)) models are predictive enough to be used as guides in designing new molecules.

Table 3
Comparison between the experimental and predicted activities (pIC_{50}) of the training set compounds for CoMFA and CoMSIA models.

Compounds	Experimental pIC_{50}	CoMFA		CoMSIA[a]	
		Predicted pIC_{50}	Residual	Predicted pIC_{50}	Residual
1	5.61	5.71	−0.10	5.62	−0.01
2	6.50	6.49	0.01	6.84	−0.34
3	6.46	6.62	−0.16	6.52	−0.06
4	6.31	6.47	−0.16	6.07	0.24
6	6.60	6.76	−0.16	6.66	−0.06
7	5.55	5.31	0.31	5.41	0.14
8	4.18	4.31	−0.13	4.72	−0.54
10	5.56	5.72	−0.16	5.84	−0.28
11	6.56	6.64	−0.08	6.73	−0.17
12	6.66	6.50	0.16	6.28	0.38
14	6.14	5.80	0.35	5.76	0.38
15	6.74	7.07	−0.33	7.04	−0.30
16	5.44	5.61	−0.17	5.71	−0.27
17	6.33	6.49	−0.16	6.61	−0.28
18	6.29	6.34	−0.05	6.13	0.16
20	5.46	5.63	−0.17	5.64	−0.18
21	7.41	6.94	0.74	6.91	0.50
22	6.35	5.84	0.51	5.56	0.79
24	6.45	6.60	−0.13	6.77	−0.32
25	6.51	6.66	−0.05	6.40	0.11
27	6.51	6.40	0.11	6.56	−0.05
28	7.55	7.57	−0.02	7.44	0.11
29	7.72	7.40	0.32	7.49	0.23
30	7.62	7.79	−0.17	7.73	−0.11
32	7.40	7.48	−0.08	7.46	−0.06
33	8.40	8.36	0.04	8.36	0.04
34	7.22	7.22	0.00	7.23	−0.01
35	6.72	6.71	0.01	6.76	−0.04
36	6.38	6.35	0.03	6.31	0.07
38	8.40	8.35	0.05	8.41	−0.01
40	7.30	7.30	0.00	7.35	−0.05
41	6.43	6.47	−0.04	6.41	0.02

[a] Generated by combination of steric, electrostatic and hydrophobic fields.

3.3. Contour map analyses

As described in Section 2.1, the best CoMFA model was generated by combination of steric (S) and electrostatic (E) fields whereas a combination of steric (S), electrostatic (E) and hydrophobic (H) fields were used to generate the best CoMSIA model (Table 2). In both cases the field contributions were represented by a default 'STDDEV*COEFF' contour maps of different color-coded regions that aid in the visualization of favored and disfavored interactions of ligands with protein targets. The maps surround all lattice points where the QSAR is found to strongly associate changes in the molecular field values with the corresponding changes in binding affinity or any other measurable bioactivity. They were generated as a scalar product of coefficients and the standard deviations associated with each column of CoMFA and CoMSIA. In this section the respective contour map analyses of the CoMFA and CoMSIA models are presented.

Table 4
Comparison between the experimental and predicted activities (pIC_{50}) of the test set compounds for CoMFA and CoMSIA models.

Compounds	Experimental pIC_{50}	CoMFA		CoMSIA[a]	
		Predicted pIC_{50}	Residual	Predicted pIC_{50}	Residual
5	6.64	6.62	0.02	6.39	0.25
9	7.36	7.05	0.31	6.83	0.53
13	6.60	6.64	−0.04	6.60	0.00
19	6.82	6.50	0.32	6.47	0.35
23	6.00	5.78	0.22	5.19	0.81
26	6.53	6.51	0.02	6.50	0.03
31	7.54	7.68	−0.14	7.77	−0.23
37	6.41	7.25	−0.84	7.23	−0.82
39	8.40	7.82	0.58	7.87	0.53
42	6.74	7.02	−0.28	7.19	−0.45

[a] Generated by combination of steric, electrostatic and hydrophobic fields.

3.3.1. Visual inspection of 3D contour maps generated by CoMFA

The CoMFA steric and electrostatic maps of cycloguanil-derivatives used in the study are depicted in Fig. 6 along with the most active compound (**38**) displayed in the background. In these contour maps, the green contours show the regions where sterically bulkier groups are associated with increase in biological activity. On the other hand, yellow contours indicate the regions where such bulkier groups lower biological activities of ligands [45]. For the selected best CoMFA model, green contours were observed near 3′-substituent of 5-aryl ring and at about three C–C bonds away from C6 atom of the 1,3,5-triazine ring (Fig. 6(a)). No yellow-colored contour was observed in this model. The green regions show that increasing steric bulk at these positions results in increased bioactivities of cycloguanil-derivatives. This is consistent with the fact that those compounds with higher pIC_{50} values bear bulky substituents either at C6- or the *meta*-position of the 5-aryl ring. Some compounds also have bulky substituents at both positions. For the sake of systematic discussion of the effect of steric bulk on bioactivities, the molecules used in this study were classified into the following four sub-classes. These are (i) **26**–**29**, (ii) **6**, **9**, **15**, **21**, **32** and **36**, (iii) **30**, **31**, **33–35** and **37–42** and (iv) **1**–**5**, **7**, **8**, **10**–**14**, **16**–**19** and **20**, **22**–**25**. The compounds in the first sub-class are characterized by a steric bulk group (Cl substituent) near the green contour at the 3′-position of the 5-aryl ring. **28** and **29** bear only one methyl substituent at their C6-positions, and show better anti-plasmodial activities compared to cycloguanil (**1**) as demonstrated by their high pIC_{50} values of 7.55 and 7.72, respectively. Though it has two Cl substituents at 3′- and 4′-positions, **29** has high activity. This observation could be attributed to the fact that the 3′-Cl substituent favorably interact with the enzyme's active site to enhance inhibitory activity and help to reduce the unfavorable effect of 4′-Cl substituent. **27** and **26** show moderate activities with pIC_{50} values of 6.51 and 6.53, respectively. The relatively lower activities of the latter could be attributed to the steric interaction between one of the C6-methyl groups of the triazine ring with the side chain of valine residue in the A16V + S108T mutant enzyme. Several modelling studies and *in vitro* binding assay experiments revealed that A16V mutation causes a dramatic loss in binding interaction of cycloguanil in the active site of *Pf*DHFR enzyme carrying this mutation [29–31,35]. The second sub-class of molecules (**6**, **9**, **15**, **21**, **32** and **36**) have only one bulky aryl (aliphatic) substituent group at C6-position of their 1,3,5-triazine rings which falls in the green region, and substituents such as Cl, Br and CH_3 at 4′-positions. They show moderate to high activities (Tables 3 and 4). Their anti-plasmodial activities (pIC_{50} values) are comparable to those of compounds discussed in the previous subclass. This indicated that steric bulks at the 3′-position of 5-aryl ring and the C6-position of 1,3,5-triazine ring are equally important in increasing anti-plasmodial activities.

Compounds which belong to sub-class (iii) (**30**, **31**, **33–35** and **37–42**) have sterically bulky substituents (Cl) at the 3′-position and only one bulky aliphatic/aryl groups at the C6-position. These compounds are generally potent growth inhibitors of the *P. falciparum* clone harboring the A16V + S108T mutant DHFR enzyme. The activities of molecules **35**, **37**, **41** and **42** are relatively lower as compared to the most active compounds (**33**, **34** and **39**). Further substitution in the *para*-position of the C6-aryl substituents (**33** and **34**) and/or very long aliphatic chain at C6-position (**39**) could be a reason for higher activities in the latter compounds. The pIC_{50} values of compounds in subclass (iii) are in the range of

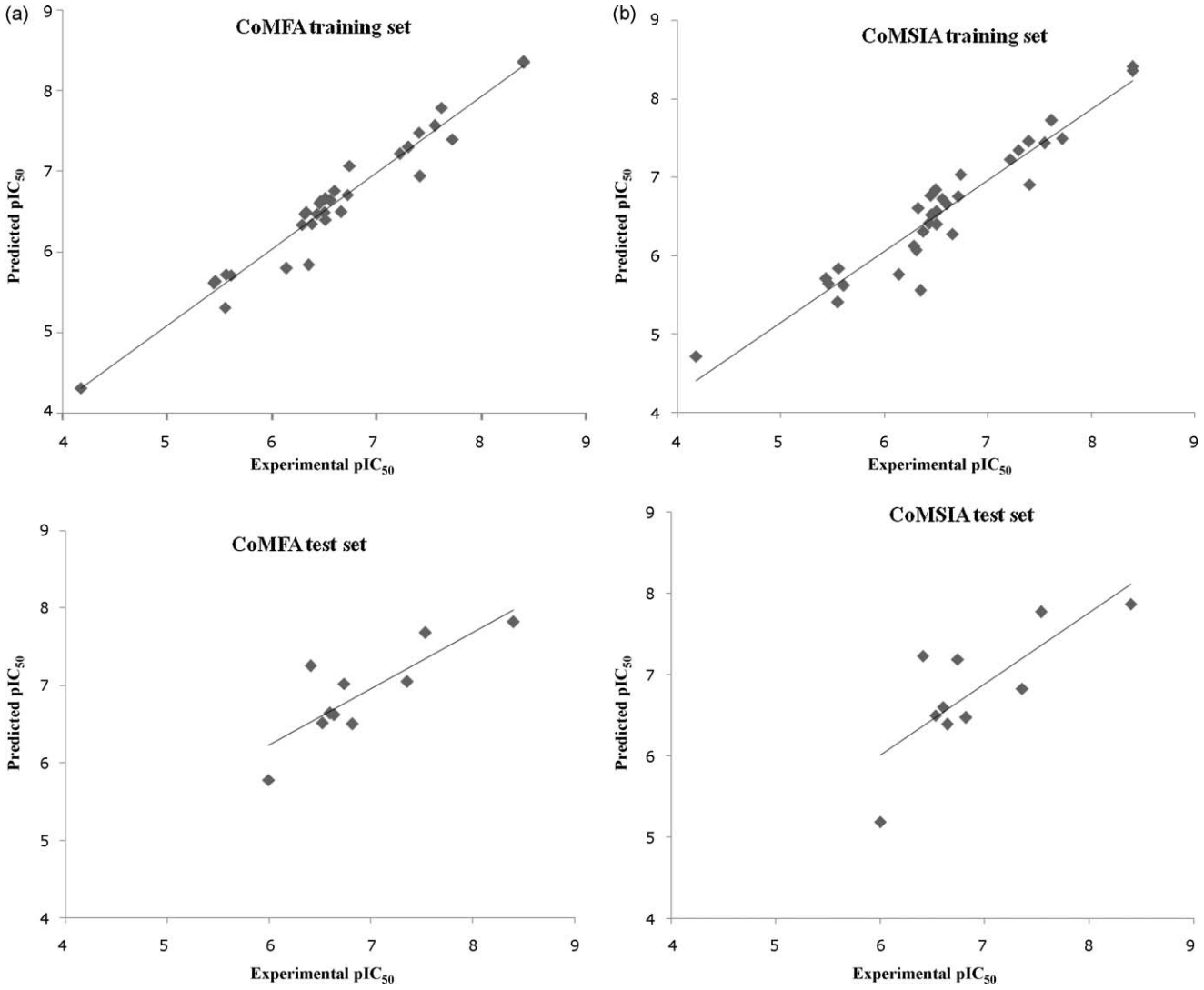

Fig. 5. Graphs of predicted versus experimental pIC_{50} values of training and test set molecules: (a) CoMFA graphs of training and test sets; (b) CoMSIA graphs of training and test sets.

6.72–8.40 (Tables 3 and 4). Comparison of the activities of this sub-class of compounds with that of compounds in subclasses (i) and (ii), demonstrated that existence of two bulky substituents in the same compound in both green regions generally enhances inhibitory activity. This observation is consistent with a hypothesis stating that relief of steric effects around residues 16 and 108 by replacing one of the methyl group of cycloguanil by hydrogen and by moving the 4′-Cl substituent to 3′-position, respectively, enhance inhibitory activities of cycloguanil derivatives against A16V + S108T mutant *Pf*DHFR enzyme. On the other hand, compounds which belong to sub-class (iv), including cycloguanil itself (**1**), have no sterically bulky substituents falling in the above-mentioned green regions. These compounds generally exhibit low activities ($pIC_{50} < 6.50$). Even though they have *tert*-butyl and isopropyl substituents at C6-position of the triazine ring, compounds **7**, **8**, **14** and **20** show low activities. This could be attributed to the fact that the bulky groups do not fall into the green region. To fall into this region, the length of the bulky group should be about three C–C bonds away from the 1,3,5-triazine ring (or C6 atom) and also another group should be located at 3′-position of 5-aryl ring of cycloguanil derivatives (Fig. 6(a)). It is important to note that compounds with no bulky substituents at both 1,3,5-triazine ring and 5-aryl side chain (e.g., **24**) show comparatively low inhibitory activities as compared to those compounds in sub-class (iii). This fact supports our argument that states consistent with the CoMFA steric contour maps, a compound should possess one steric bulk group at C6-position and another at 3′-position of cycloguanil analog to be effective inhibitor of A16V + S108T mutant *Pf*DHFR enzyme. This observation also suggests that compounds with substituents at these positions might interact favorably with the enzyme's active site to enhance inhibitory activities.

The CoMFA electrostatic interaction contour maps (Fig. 6(b)) are represented by red and blue regions. The red contours represent regions where electron-rich (electronegative) groups result in enhanced bioactivity whereas blue contours correspond to regions where increased positive charge (or decreased negative charge) would result in an enhanced biological activity. Three small red contours near 3′-Cl substituent, and other two small red contours on C6-substituent at about C–C length distance from C6 atom were observed (Fig. 6(b)). The most active compounds (**33**, **38** and **39**) and other compounds in subclass (iii) have red contour maps near an electronegative substituent (Cl) at the 3′-position. Comparison of the activities of **1** vs. **26**, **33** vs. **32**, and **36** vs. **37** demonstrated that an electronegative Cl substituent at the 3′-position could contribute to the observed high activities of these

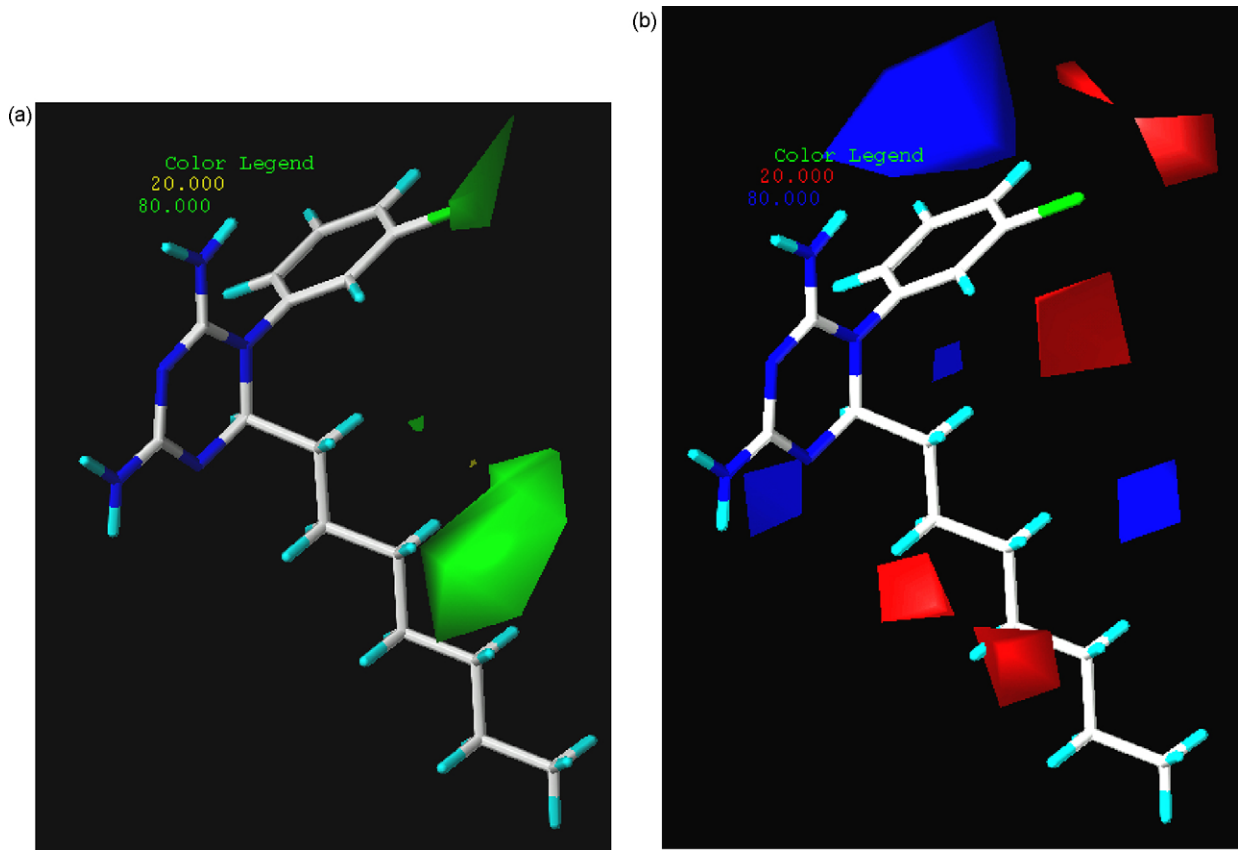

Fig. 6. STDDEV*COEFF plots of the CoMFA steric (a) and electrostatic (b) contour maps. The most active molecule (**38**) is displayed in the background. Green region: sterically favored; yellow region: sterically disfavored; red region: negatively charged favored; blue region: positively charged favored.

compounds. Hence, higher activities of **26**, **33** and **37** could be attributed to the presence of 3′-Cl substituent that fall into the red region. Most of these compounds also have aryloxy substituent groups at the C6-position which is closer to the second group of red contour maps. This is also consistent with high activities of **34**–**37** and **40**–**42**. As demonstrated by the pIC_{50} values, the presence of electron electronegative substituents such as chlorine (**1**–**5**, **7** and **8**), bromine (**10**–**14**), and fluorine (**15** and **23**) at the 4′-position of the aryl ring did not increase activities of these cycloguanil analogs. This is because they are not located in the red contour region which is closer to 3′-position (Fig. 6(b)). Another possible reason is that 4′-Cl or other bulky substituents at the 4′-position encounter unfavorable steric clashes due to bulky side chain of T108 in the active site of A16V + S108T mutant *Pf*DHFR enzyme (Section 3.2) [20,26,29–31,35,37,64]. These are the most probable reasons why most of the compounds with bulky substituent groups at the 4′-position show low pIC_{50} values (Table 1). Blue contours represent regions where increased positive charge (or decrease negative charge) would result in enhanced activity. In the CoMFA model, one big blue contour (Fig. 6(b)) near 5′-position of the aryl ring, and a group of other small blue contour maps one near N1- and C6-substituents were observed. The maps indicated that introduction of electropositive groups at these positions would increase anti-plasmodial activities of cycloguanil derivatives. In this study no compound was found to possess an electron-deficient substituent near the blue regions. The analysis of the CoMFA contour maps also indicated that the most active compounds have bulky and electronegative substituents or at least one of them properly oriented, respectively, at the sterically and electrostatically favorable regions. Occurrence of the green and red contours together suggests the need of both sterically bulky and electron-rich substituents in order to increase inhibitory activities of cycloguanil analogues.

3.3.2. *Visual inspection of 3D-contour maps generated by CoMSIA*

The CoMSIA model was generated by combination of three physicochemical properties, viz. steric (S), electrostatic (E) and hydrophobic (H) fields (Table 2). From the direct comparison of Figs. 6 and 7, it is possible to observe some similarities and differences among the contour maps of the CoMFA and CoMSIA models. Firstly, in the case of steric maps, there is no yellow contour in the CoMFA model to indicate regions where steric bulk is not required to increase activity whereas in the CoMSIA model a group of small yellow contours were observed near C6-position of the 1,3,5-triazine ring. Green contours indicate regions where steric bulk increases activity. In both models there are big green contours located on the C6-aliphatic substituent of compound **38**. These contours are of almost equal size but with a slight difference in their location on the aliphatic side chain. The CoMFA model also has additional small green contours near 3′-Cl substituents. Secondly, comparison of the electrostatic contour maps of the CoMSIA and CoMFA models also indicated the presence of some similarities between the contour maps. Though there is difference in size and number, blue contours were observed near/on the traizine ring and near 4′-Cl group in both models. Red contours indicate regions where electron-rich groups increase activity. Only one big red contour map was observed in the CoMSIA model near C6-atom (Fig. 7(b)) whereas a group of small red contours were observed in the CoMFA model near 3′-Cl substituent and C-6 substituent of compound **38** (Fig. 6(b)). This is consistent with reports revealing that inhibitory activities of cycloguanil analogues could be enhanced by moving Cl substituent from *para*-position to

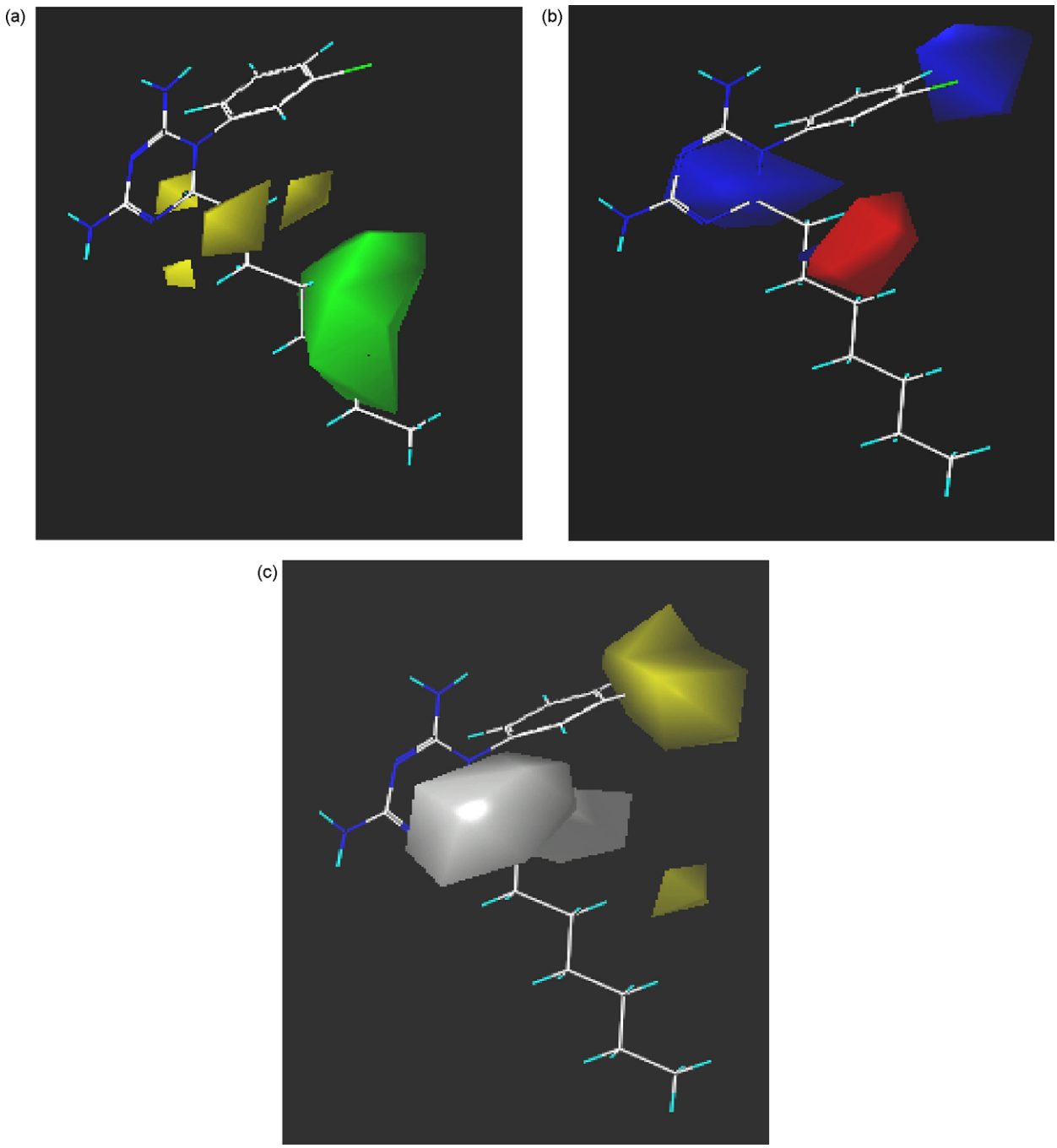

Fig. 7. The CoMSIA steric (Fig. 4(a)) and electrostatic (Fig. 4(b)) contour maps and hydrophobic field (Fig. 4(c)). Green region: sterically favored; yellow region: sterically disfavored; red region: negatively charged favored; blue region: positively charged favored; yellow region: favored; white: disfavored). The most active compound **38** is shown in the background.

meta-position [29,30]. Because of several similarities among the steric and electrostatic contour maps with the corresponding maps of the CoMFA model, details of steric and electrostatic contours of the CoMSIA model are not discussed here.

The hydrophobic contour map of the CoMSIA model is shown in Fig. 7(c) with the most active compound (**38**) displayed in the background. White contours indicate that regions where hydrophobic substituents decrease activities of compounds whereas the yellow contours indicate regions where hydrophobic substituents increase activities of compounds. White contours were located on and near the 1,3,5-triazine ring of **38**. This indicates that hydrophobicity is not required in these regions particularly near N1 of the triazine ring. It is well known that N1 gets protonated at physiological pH in order to form a bidentate H-bond interaction with the conserved acid residue (Asp54) in the active site of *Pf*DHFR enzyme. Such H-bonding interactions are known to be essential for *Pf*DHFR inhibitory activities of antifolates such as cycloguanil [19,31–33]. Hence, hydrophobicity needs to be reduced near the 1,3,5-triazine ring to enhance anti-plasmodial activities of cycloguanil analogues. This can be done by introducing alkoxy or aryloxy groups at C6-position. On the other hand, a big yellow contour was observed near the 5-phenyl ring indicating that hydrophobicity is required in this region to increase activity. This contour is found near the 3′-Cl substituent of the template molecule (**38**) suggesting significant contribution of 3′-Cl substituent to the hydrophobic interaction thereby increasing

inhibitory activity. This is further supported by observed high experimental inhibitory activities of **28**–**31**, **33**–**35**, **38**, **39** and **40**. All these compounds bear 3′-Cl substituents and their pIC_{50} values are >7.30.

4. Conclusions

The main objective of this study was to develop statistically robust CoMFA and CoMSIA models with good correlation and predictive powers using anti-plasmodial activity data of cycloguanil derivatives. Thus, the models were generated from a training set composed of 32 compounds for which their growth inhibitory activities were tested against *P. falciparum* clone (T9/94 RC17) harboring A16V + S108T mutant DHFR enzyme. The CoMFA model was found to give better result as demonstrated by its statistical indices ($r^2_{cv} = 0.654$, $r^2_{ncv} = 0.951$, $r^2_{bs} = 0.974$ and $r^2_{pred} = 0.735$) which were relatively better than the corresponding indices ($r^2_{cv} = 0.669$, $r^2_{ncv} = 0.907$, $r^2_{bs} = 0.967$ and $r^2_{pred} = 0.557$) of the CoMSIA model.

The constructed 3D-QSAR models and structure activity relationship (SAR) analyses of the compounds used in the study suggested that an electronegative and bulky substituent at 3′-position and one bulky substituent at C6-position of cycloguanil analogs are required to design novel inhibitors of A16V + S108T mutant *Pf*DHFR enzyme.

Acknowledgements

Legesse Adane Bahiru is thankful to the government of Federal Democratic Republic of Ethiopia for financial support.

Appendix A. Supplementary data

Supplementary data associated with this article can be found, in the online version, at doi:10.1016/j.jmgm.2009.09.001.

References

[1] S. Nwaka, A. Hudson, Innovative lead discovery strategies for tropical diseases, Nat. Rev. Drug Discov. 5 (2006) 941–955.
[2] R.S. Philips, Current status of malaria and potential control, Clin. Microbiol. Rev. 14 (2001) 208–226.
[3] J.K. Baird, Effectiveness of antimalarial drugs, New Engl. J. Med. 352 (2005) 1565–1577.
[4] P. Winstaly, S. Ward, R. Snow, A. Breckenridge, Therapy of falciparum malaria in Sub-Saharan Africa: from molecule to policy, Clin. Microbiol. Rev. 17 (2004) 612–637.
[5] D.A. Fidock, P.J. Rosenthal, S.L. Croft, R. Brun, S. Nwaka, Antimalarial drug discovery; efficacy model for compound screening, Nat. Rev. Drug Discov. 3 (2004) 509–520.
[6] R.G. Ridley, Medical need, scientific opportunity and the drive for antimalarial drugs, Nature 415 (2002) 686–693.
[7] WHO expert committee on malaria, Technical report series, Twentieth report, WHO, Geneva, 2000.
[8] J. Sachs, P. Malaney, The economic and social burden of malaria, Nature 41 (2002) 680–685.
[9] O.A. Talisuna, P. Bloland, U. D'Alessandro, History, dynamics and public health importance malaria parasite, Clin. Microbiol. Rev. 17 (2004) 235–254.
[10] P.B. Bloland, Drug Resistance in Malaria, WHO, 2001.
[11] N.J. White, Antimalarial drug resistance, J. Clin. Infect. 113 (2004) 1084–1092.
[12] A. Gregson, C.V. Plowe, Mechanism of resistance of malaria parasites to antifolates, Pharmacol. Rev. 57 (2005) 117–140.
[13] Y.D. Sharma, Genetic alteration in drug resistance markers of *P. falciparum*, Ind. J. Med. Res. 121 (2005) 13–22.
[14] P. Ollario, Drug resistance hampers our capacity to roll back malaria. antimalarial drug resistance, Clin. Infect. Dis. 41 (2005) S247–S257.
[15] I.M. Kompis, K. Islam, R.L. Then, DNA and RNA synthesis: antifolates, Chem. Rev. 105 (2006) 593–620.
[16] A.C. Anderson, Targeting DHFR in parasitic protozoa, Drug Discov. Today 10 (2005) 121–128.
[17] E.F. Da Cuhan, T.C. Ramlho, E.R. Maia, R.B. de Alenncastro, The search for new DHFR inhibitors: a review of patents, January 2001–February 2005, Expert. Opin. Ther. Patents 15 (2005) 1–20.
[18] P.D. Braun, K.T. Barglow, Y.M. Lin, T. Akompong, R. Briesewitz, G.T. Ray, K. Haldar, T.J. Wandless, A bifunctional molecule that displays context-dependent cellular activity, J. Am. Chem. Soc. 125 (2003) 7575–7580.
[19] T.C.C. França, A.L.R. de Medeiros, E.C.P. dos Santos, O.A. Santos-Filho, J.D.A. Figueroa-Villar, A Complete homology model of the *P. falciparum* bifunctional enzyme dihydrofolate reductase-thymidylate synthase. a model to design new antimalarials, J. Braz. Chem. Soc. 15 (2004) 450–454.
[20] R.T. Delfino, O.A. Santos-Filho, J.D. Figueroa-Villar, Type 2 antifolates in the chemotherapy of falciparum malaria, J. Braz. Chem. Soc. 15 (2004) 727–741.
[21] R.T. Delfino, O.A. Santos-Filho, J.D. Figueroa-Villar, Molecular modeling of wild-type and antifolate resistant mutant *P. falciparum* DHFR, Biophys. Chem. 98 (2002) 287–300.
[22] P.K. Rathod, M.A. Philips, Prized malaria drug target nailed, Nat. Struct. Biol. 10 (2003) 316–318.
[23] J. Yuvaniyama, P. Chitnumsub, S. Kamchonwongpaisan, J. Vanichatanankul, W. Sirawaraporn, P. Taylor, M.D. Walkinshaw, Y. Yuthavong, Insights into antifolate resistance from malarial DHFR-TS structures, Nat. Struct. Biol. 10 (2003) 357–365.
[24] A. Nzila, Inhibitors of *de novo* folate enzymes in *P. falciparum*, Drug Discov. Today 11 (2006) 939–944.
[25] O.A. Santos-Filho, R.D. de Alencastrob, J.D. Figueroa-Villar, Homology modeling of wild-type and pyrimethamine/cycloguanil-cross-resistant mutant type *P. falciparum* DHFR: a model for antimalarial chemotherapy resistance, Biophys. Chem. 91 (2001) 305–317.
[26] D.C. Warhurst, Resistance to antifolates in *P. falciparum*, the causative agent of tropical malaria, Sci. Prog. 85 (2002) 89–111.
[27] D.S. Peterson, W.K. Milhous, T.E. Wellems, Molecular basis of differential resistance to cycloguanil and pyrimethamine in *P. falciparum* malaria, Proc. Natl. Acad. Sci. U.S.A. 87 (1990) 3018–3022.
[28] W. Sirawaraporn, T. Sathitkul, R. Sirawaraporn, Y. Yuthavong, D.V. Santi, Antifolate-resistant mutants of *P. falciparum* dihydrofolate reductase, Proc. Natl. Acad. Sci. U.S.A. 94 (1997) 1124–1129.
[29] G. Rastelli, W. Sirawaraporn, P. Sompornpisut, T. Vilaivan, S. Kamchonwongpaisan, R. Quarrell, G. Lowe, Y. Thebtaranonth, Y. Yuthavong, Interaction of pyrimethamine, cycloguanil, WR99210 and their analogues with *Pf*DHFR: structural basis of antifolate, Bioorg. Med. Chem. 8 (2000) 1117–1128.
[30] T. Lemcke, I.T. Christensen, F.S. Jorgensen, Towards understanding of drug resistance in malaria: three-dimensional structure of *P. falciparum* DHFR by homology building, Bioorg. Med. Chem. 7 (1999) 1003–1011.
[31] D.V. Warhurst, Antifolate drug discovery: development of inhibitors of DHFR active in drug resistance, Drug Discov. Today 3 (1998) 538–546.
[32] M.D. Parenti, S. Pacchioni, A.M. Ferrari, G. Rastelli, Three-dimensional quantitative structure–activity relationship analysis of a set of *P. falciparum* dihydrofolate reductase inhibitors using a pharmacophore generation approach, J. Med. Chem. 47 (2004) 4258–4267.
[33] G. Rastelli, S. Pacchioni, W. Sirawaraporn, R. Sirawaraporn, M.D. Parenti, A.M. Ferrari, Docking and database screening reveal new classes of *P. falciparum* dihydrofolate reductase inhibitors, J. Med. Chem. 46 (2003) 2834–2845.
[34] C. Portela, C.M. Afonso, M.M. Pinto, M.J. Ramos, Computational studies of new potential antimalarial compounds—stereoelectronic complementarity with the receptor, J. Comput.-Aided Mol. Des. 17 (2003) 583–595.
[35] Y. Yuthavong, T. Vilainvan, N. Chareonsethakul, S. Kamchonwongpaisan, W. Sirawaraporn, R. Quarrell, G. Lowe, Development of a lead inhibitor for the A16V + S108T mutant of DHFR from cycloguanil-resistant strain (T9/94) of *P. falciparum*, J. Med. Chem. 43 (2000) 2738–2744.
[36] S. Kamchonwongpaisan, R. Quarrell, N. Charoensetakul, R. Ponsinet, T. Vilaivan, J. Vanichtananankul, B. Tarnchompoo, W. Sirawaraporn, G. Lowe, Y. Yuthavong, Inhibitors of multiple mutants of *P. falciparum* DHFR and their antimalarial activities, J. Med. Chem. 47 (2004) 673–680.
[37] F. Cheng, J. Shen, X. Luo, W. Zhu, J. Gu, R. Ji, H. Jiang, K. Chen, Molecular docking and 3D-QSAR studies on the possible antimalarial mechanism of artemisinin analogues, Bioorg. Med. Chem. 10 (2002) 2883–2891.
[38] O.A. Santos-Filho, A.J. Hopfinger, A search for sources of drug resistance by the 4D-QSAR analysis of a set of antimalarial dihydrofolate reductase inhibitors, J. Comput.-Aided Mol. Des. 15 (2001) 1–12.
[39] O.A. Santos-Filho, R.K. Mishra, A.J. Hopfinger, Free energy force field (FEFF) 3D-QSAR analysis of a set of *P. falciparum* dihydrofolate reductase inhibitors, J. Comput.-Aided Mol. Des. 15 (2001) 787–810.
[40] D. Hecht, M. Cheung, G.B. Fogel, QSAR using evolved neural networks for the inhibition of mutant *Pf*DHFR by pyrimethamine derivatives, Biosystems 92 (2008) 10–15.
[41] D.A. Winkler, The role of quantitative structure–activity relationships (QSAR) in biomolecular discovery, Brief. Bioinform. 3 (2002) 73–86.
[42] M.A. Lill, Multi-dimensional QSAR in drug discovery, Drug Discov. Today 12 (2007) 1013–1017.
[43] R.C. Wade, S. Henrich, T. Wang, Using 3D protein structures to derive 3D-QSARs, Drug Discov. Today: Technol. 1 (2004) 241–246.
[44] A. Hillebrecht, G. Klebe, Use of 3D-QSAR models for database screening: a feasibility study, J. Chem. Inform. Model. 48 (2008) 384–396.
[45] R.D. Cramer, D.E. Patterson, J.D. Bunce, Effect of shape on binding of steroids to carrier proteins, J. Am. Chem. Soc. 110 (1988) 5959–5967.
[46] G. Klebe, U. Abraham, T. Mietzner, Molecular similarity indices in a comparative analysis (COMSIA) of drug molecules to correlate and predict their biological activity, J. Med. Chem. 37 (1994) 4130–4146.
[47] P. Maitarad, S. Hannongbua, S. Kamchonwongpaisan, J. Vanichtananankul, T. Vilaivan, T. Yuthavong, Interactions between cycloguanil derivatives and wild type

and resistance-associated mutant *P. falciparum* dihydrofolate reductases, J. Comput.-Aided. Mol. Des. 23 (2009) 241–252.
[48] P. Maitarad, P. Saparpakorn, S. Hannongbua, S. Kamchonwongpaisan, B. Tarnchompoo, Y. Yuthavong, Particular interaction between pyrimethamine derivatives and quadruple mutant type dihydrofolate reductase of *P. falciparum*: CoMFA and quantum chemical calculations studies, J. Enzyme Inhib. Med. Chem. 24 (2009) 471–479.
[49] SYBYL6.9, Tripose Inc., 1699 S. Hanley Rd., St. Louis, MO 631444, USA.
[50] A.K. Chakraborti, B. Gopalakrishnan, M.E. Sobhia, A. Malde, 3D-QSAR studies of indole derivatives as phosphodiesterase IV inhibitors, Eur. J. Med. Chem. 38 (2003) 975–982.
[51] T.L. Aboye, M.E. Sobhia, P.V. Bharatam, 3D-QSAR studies of pyruvate dehydrogenase kinase inhibitors based on a divide and conquer strategy, Bioorg. Med. Chem. 12 (2004) 2709–2715.
[52] C.M. Avila, N.C. Romeiro, G.M. da Silva, C.M. Sant'Anna, E.J. Barreiro, C.A. Fraga, Development of new CoMFA and CoMSIA 3D-QSAR models for anti-inflammatory phthalimide-containing TNFalpha modulators, Bioorg. Med. Chem. 14 (2006) 6874–6885.
[53] P.S. Kumar, P.V. Bharatam, CoMFA study on selective human β3-adrenoreceptor agonists, in: ARKIVOC, XIII, 2005, 67–69.
[54] G.M. Morris, D.S. Goodsell, R. Huey, A.J. Olson, Distributed automated docking of flexible ligands to proteins: parallel applications of AutoDock 2.4, J. Comput.-Aided Mol. Des. 10 (1996) 293–304.
[55] O.M.H. Salo, J.R. Savinainen, T. Parkkari, T. Nevalainen, M.J. Kakkonen, J. Gynther, J.T. Laitinen, T. Järvinen, A. Poso, 3D-QSAR studies on cannabinoid CB1 receptor agonists: G-protein activation as biological data, J. Med. Chem. 49 (2006) 554–566.
[56] M.T. Barakat, P.M. Dean, Molecular structure matching by simulated annealing. I. A comparison between different cooling schedules, J. Comput.-Aided Mol. Des. 4 (1990) 295–316.
[57] J. Gasteiger, M. Marsili, Iterative partial equalization of orbital electronegativity—a rapid access to atomic charges, Tetrahedron 36 (1980) 3219–3228.
[58] W. Sippl, Development of biologically active compounds by combining 3D-QSAR and structure-based design methods, J. Comput.-Aided Mol. Des. 16 (2002) 825–830.
[59] S. Wold, Validation of QSAR's, Quant. Struct.-Act. Relat. 10 (1991) 191–193.
[60] R.D. Cramer, J.D. Bunce, D.E. Patterson, I.E. Frank, Cross-validation, bootstrapping, and partial least squares compared with multiple regression in conventional QSAR studies, Quant. Struct.-Act. Relat. 7 (1988) 18–25.
[61] V.S. Murthy, V.M. Kulkarni, 3D-QSAR CoMFA and CoMSIA on protein tyrosine phosphatase 1B inhibitors, Bioorg. Med. Chem. 10 (2002) 2267–2282.
[62] A. Golbraikh, A. Tropsha, Beware of q2, J. Mol. Graph. Model. 20 (2002) 269–276.
[63] A. Tropsha, T. Oprea, Chemoinformatics in Drug Discovery, Wiley, Weinheim, 2005, p. 437.
[64] B. Tarnchompoo, C. Sirichaiwat, W. Phupong, C. Intaraudom, W. Sirawaraporn, S. Kamchonwongpaisan, J. Vanichtanankul, Y. Thebtaranonth, Y. Yuthavong, Development of 2,4-diaminopyrimidines as antimalarials based on inhibition of the S108N and C59R + S108N mutants of dihydrofolate reductase from pyrimethamine-resistant *P. falciparum*, J. Med. Chem. 45 (2002) 1244–1252.